Journal of Zhejiang University-SCIENCE B (Biomedicine & Biotechnology) *2025 26(1):92-106*
www.jzus.zju.edu.cn; www.springer.com/journal/11585
E-mail: jzus_b@zju.edu.cn

Research Article
https://doi.org/10.1631/jzus.B2400192

CXCL16 promotes proliferation of head and neck squamous cell carcinoma by regulating GPX1-mediated antioxidant levels

Ru HE[1*], Hongyi JIANG[1,6*], Chengchi ZHANG[2], Yuan CHEN[3], Wenshun LIU[4], Xinyue DENG[1,6], Xiaozheng ZHU[1,6], Yunye LIU[1], Chuanming ZHENG[1,6], Yining ZHANG[5], Chengying SHAO[5], Yanting DUAN[1,6✉], Jiajie XU[1,6✉]

[1]*Otolaryngology & Head and Neck Center, Cancer Center, Department of Head and Neck Surgery, Zhejiang Provincial People's Hospital (Affiliated People's Hospital), Hangzhou Medical College, Hangzhou 310014, China*
[2]*College of Biotechnology and Bioengineering, Zhejiang University of Technology, Hangzhou 310014, China*
[3]*Cancer Center, Department of Pathology, Zhejiang Provincial People's Hospital (Affiliated People's Hospital), Hangzhou Medical College, Hangzhou 310014, China*
[4]*Department of Postgraduate Education, Jinzhou Medical University, Jinzhou 121000, China*
[5]*The Second School of Clinical Medicine, Zhejiang Chinese Medical University, Hangzhou 310053, China*
[6]*Zhejiang Key Laboratory of Precision Medicine Research on Head & Neck Cancer, Hangzhou 310014, China*

Abstract: Numerous studies have demonstrated that the high expression of CXC motif chemokine ligand 16 (CXCL16) in cancer correlates with poor prognosis, as well as tumor cell proliferation, migration, and invasion. While CXCL16 can serve as a tumor biomarker, the underlying mechanism in modulating head and neck squamous cell carcinoma (HNSCC) remains unclear. In this study, the aimed was to investigate the CXCL16 expression in HNSCC and to uncover the potential underlying mechanism. Hereby, we determined the high expression of CXCL16 in The Cancer Genome Atlas (TCGA) database, as well as in tissue samples from patients with HNSCC at our central hospital and from HNSCC cell lines. The results showed that *CXCL16* knockdown inhibited the proliferation, migration, and invasion of HNSCC cells. Mechanistically, transcriptome sequencing revealed that CXCL16 may affect HNSCC cell growth by regulating the antioxidant pathway of glutathione peroxidase 1 (GPX1). The reactive oxygen species (ROS) levels were elevated in small interfering CXCL16 (si-CXCL16) cells, which may contribute to the inhibition of cell proliferation, migration, and invasion. Moreover, treatment of cells with the GPX1 inhibitor eldecalcitol (ED-71) revealed that HNSCC cell growth was significantly inhibited in the synergistic group of si-CXCL16 and GPX1 inhibitor compared to the si-CXCL16 group. In conclusion, CXCL16 contributed to the development of HNSCC cells by modulating the GPX1-mediated antioxidant pathway. Thus, targeting cellular CXCL16 expression seems to be a promising strategy for treating HNSCC.

Key words: Antioxidant pathway; CXC motif chemokine ligand 16 (CXCL16); Glutathione peroxidase 1 (GPX1); Head and neck squamous cell carcinoma (HNSCC)

1 Introduction

Head and neck squamous cell carcinoma (HNSCC), originating from the squamous mucosa of the upper aerodigestive tract, including the nasal cavity, nasopharynx, larynx, hypopharynx, and oropharynx, is ranked sixth among cancer-related deaths worldwide, with over 350 000 new cases and 170 000 deaths reported annually (Fan et al., 2011; Bray et al., 2018; Siegel et al., 2020). While diagnosis and multimodal treatment of HNSCC have recently shown rapid advancement, the 5-year survival rate remains low because of the complex anatomy of the head and neck (Brockstein et al., 2004). Cancer immunotherapy has gained widespread study and use in clinical settings in recent years, leading to significant changes in HNSCC treatment. For example, checkpoint inhibitors targeting

✉ Yanting DUAN, dyt19880818@163.com
Jiajie XU, xujiajie@hmc.edu.cn
* The two authors contributed equally to this work
Ru HE, https://orcid.org/0000-0002-9712-3386
Hongyi JIANG, https://orcid.org/0009-0005-1696-9160
Jiajie XU, https://orcid.org/0000-0001-5539-3831

Received Apr. 15, 2024; Revision accepted July 29, 2024;
Crosschecked Sept. 4, 2024; Published online Sept. 30, 2024

programmed cell death protein 1 (PD-1), programmed death-ligand 1 (PD-L1), and cytotoxic T-lymphocyte antigen 4 (CTLA-4), either alone or combined with radiotherapy or chemotherapy, are being investigated in clinical trials, as are novel approaches based on cytokines or overt T-cell therapy (Mei Z et al., 2020; Moreira et al., 2021; Hsieh et al., 2022). Although these immunotherapies have demonstrated significant benefits in some patients with advanced HNSCC, because of tumor heterogeneity, the effect of immunosuppressants remains inferior compared to the initial expectations. This is evidenced by limited objective remission rate, with fewer than 20% of patients experiencing clinical benefit and the most facing poor prognosis (Siu et al., 2019; Saddawi-Konefka et al., 2022). Therefore, there is an urgent need for effective biomarkers to predict the progression of HNSCC, thus enabling accurate and efficient disease status assessment to improve prognosis and reduce mortality rates.

Chemokines, a group of factors with chemotactic properties, control the migration and localization of immune cells, playing an essential role in the movement of all immune cells (Griffith et al., 2014). CXC motif chemokine ligand 16 (CXCL16) is a CXC-soluble chemokine with its gene located on chromosome 17p13, a separate locus distinct from other known chemokines (Matloubian et al., 2000; Izquierdo et al., 2014). CXCL16 factors function in two primary forms: membrane-bound molecules and soluble chemokines (Abel et al., 2004). It has been found that soluble CXCL16 can activate the expression of transmembrane CXCL16 through homodimerization and enhance proliferation and anti-apoptotsis of tumor cells by the phosphorylation of intracellular kinases (Hattermann et al., 2016).

Among the chemokine receptors, the specific receptor for CXCL16 is CXC chemokine receptor 6 (CXCR6), which is potentially involved in metabolic disorders, inflammatory responses, and T-cell migration and recruitment in vivo through the CXCR6-CXCL16 signaling axis (Matloubian et al., 2000; Collado et al., 2018; Karaki et al., 2021). Therefore, many researchers have investigated the role of this signaling axis in cancer. It was shown to have an intimate relationship with tumor progression and poor prognosis, as CXCL16 promoted the growth, migration, and invasive ability of microglioma, thyroid, lung and gastric cancer cells, as well as epithelial–mesenchymal transition (EMT) pathway transformation (Hu et al., 2014; Cho et al., 2016; Lepore et al., 2018; Han et al., 2021). Several studies have reported that high CXCL16 expression in tumors contributes to tumor growth and invasion in the microenvironment by polarizing macrophages toward M2 and increasing angiogenesis (Kim et al., 2019). Additionally, in pancreatic ductal adenocarcinoma, deletion of growth inhibitory somatostatin receptor subtype 2 (SST2) expression activates phosphoinositide 3-kinase (PI3K), leading to activation of nuclear factor-κB (NF-κB) and Kirsten rat sarcoma viral oncogene homolog (KRAS) signaling, increased CXCL16 expression, and pancreatic tumor formation (Chalabi-Dchar et al., 2015). Although the molecular mechanism of tumor cell metastasis promotion needs to be explored further, it has been recognized that CXCL16 plays a crucial role in the onset and progression of cancer.

Glutathione peroxidase 1 (GPX1) is an essential antioxidant enzyme in cells, capable of oxidizing glutathione (GSH) to its disulfide form and maintaining cellular redox balance by regulating intracellular reactive oxygen species (ROS) levels (Zhao et al., 2022). It has been found that HNSCC patients with a higher oxidative stress glutathione disulfide (GSSG)/GSH ratio have a higher risk of local tumor recurrence rate after treatment (Dequanter et al., 2017). Therefore, studying the mechanism related to oxidative stress in HNSCC cells can provide a basis for enriching the prognosis of HNSCC patients. Eldecalcitol (ED-71), a novel active vitamin D analogue with anti-osteoporotic properties, could inhibit GPX1 expression and suppress oral cancer progression (Liu et al., 2022; Lu et al., 2023). However, chemokines associated with GPX1 in HNSCC have been rarely reported.

In our study, knockdown of *CXCL16* expression in HNSCC cells significantly downregulated the expression level of GPX1 and inhibited the antioxidant capacity of HNSCC cells, thereby suppressing their proliferation and metastatic ability. Our study provides an important basis for the stylization of CXCL16 as a candidate molecule in the diagnosis or treatment of HNSCC.

2 Materials and methods

2.1 Patients and follow-up

The selected cohort comprised 11 patients with oral squamous cell carcinoma who underwent surgery between 2022 and 2023. A total of 559 patients with

HNSCC were included in The Cancer Genome Atlas (TCGA) database.

2.2 Immunohistochemical assay

After fixation, dehydration, wax dipping, and paraffin embedding, the tissues were cut into 3-μm-thick sections and adhered to slides. Endogenous peroxides and non-specific proteins were blocked with 3% (volume fraction) hydrogen peroxide. Tissue sections were treated with primary antibodies CXCL16 (Bio-Techne, #AF976, USA) and CXCR6 (Abcepta, #AP73581, Suzhou, China) at 4 ℃ overnight. The next day, sections were washed three times and stained with secondary antibodies for 30 min at room temperature. Subsequently, the tissue sections were stained with diaminobenzidine for 3 min and nuclei were counterstained with hematoxylin for 1 min at room temperature. The CXCL16 staining scoring criteria were as follows: intensity of staining, 0–no detectable staining, 1–light yellow, 2–medium yellow, or 3–deep yellow; percentage of staining, 1 (≤10%), 2 (10%–50%), 3 (50%–80%), or 4 (≥80%).

2.3 Cell culture and transfection

HACAT cells were purchased from the National Infrastructure of Cell Line Resource (Shanghai, China) and cultured in Dulbecco's modified Eagle's medium (DMEM) containing 10% (volume fraction) fetal bovine serum (FBS; KEL Biotechnology, #KC001-01, USA) and 1% (volume fraction) penicillin/streptomycin (Cienry, #CR-15140, Huzhou, China). SCC9 and SCC25 cells were obtained from Procell Life Science & Technology Co., Ltd. (Wuhan, China) and cultured in DMEM/F12 supplemented with 10% FBS, 1% penicillin/streptomycin, and 400 ng/mL hydrocortisone (complete growth medium provided by Procell). All cell lines were cultured at 37 ℃ in a humidified incubator containing 5% CO_2 and tested for mycoplasma contamination. Small interfering RNA (siRNA) was transfected using Lipo3000 (Invitrogen, USA) at a concentration of 100 nmol/L following the manufacturer's instructions, and cell function assays were performed 24 h after transfection. The sequences of the siRNAs are listed in Table S1.

2.4 CCK-8 assay

HNSCC cells (2×10^3 cells/well) transfected with small interfering CXCL16 (si-CXCL16) were cultured in 96-well plates and cell viability was detected at 0, 1, 2, 3, and 4 d. The cell counting kit-8 (CCK-8; Vazyme Biotech Co., Ltd., Nanjing, China) consisted of 90 μL of culture medium and 10 μL of CCK-8 reagent. The mixture was kept at 37 ℃ with 5% CO_2 for 2 h, followed by incubation with a Synergy LX multi-mode reader (BioTek Instruments, USA) to measure the optical density at 450 nm (OD_{450}).

In the GPX1 inhibitor assay, different groups of HNSCC cells (2×10^3 cells/well) transfected with si-CXCL16 were cultured in 96-well plates and treated with 2 μmol/L ED-71 for 0, 24, 48, 72, and 96 h. Subsequent experiments were performed as previously described and the OD_{450} values were assayed.

2.5 Clone formation

Si-CXCL16 cells (SCC9 and SCC25) were inoculated in 12-well plates at 2000 cells/well and cultured at 37 ℃ for one week. The colony cells retained in the plates were fixed with 4% (volume fraction) methanol for 20 min and then stained with 0.5% (5 g/L) crystal violet, followed by the analysis of results.

In the GPX1 inhibitor assay, si-CXCL16 cells (SCC9 and SCC25) were inoculated in 6-well plates at 5000 cells/well, treated with 2 μmol/L ED-71 and cultured at 37 ℃ for one week, followed by the analysis of results.

2.6 Cell migration and invasion

Cell migration assays were performed using a modified Boyden chamber (Corning, #3422, USA). A total of 5×10^4 cells were suspended in 200 μL of serum-free DMEM/F12 and inoculated onto polycarbonate filters for migration assays, with each lower chamber filled with 600 μL of 10% FBS-DMEM/F12. For the invasion assay, matrix gel was diluted in serum-free DMEM/F12 at a volume ratio of 1:6, and then the formulated matrix gel was wrapped around the upper chamber membrane and incubated at 37 ℃ for 3 h. To assess the invasive ability of HNSCC, 1×10^5 cells in 200 μL of serum-free DMEM were placed into the upper chamber of wells coated with reconstituted matrix gel, while 600 μL of 10% FBS-DMEM/F12 was placed in the lower chamber. After 24 h of incubation, the cells that migrated or invaded the lower chamber were fixed with 1 mL of 4% (volume fraction) formaldehyde for 20 min and stained with 0.5% crystal violet for 30 min. Unmigrated cells in the upper chamber were

removed and the chamber was washed with phosphate-buffered saline (PBS). Each well was randomly photographed using an EVOS M7000 Smart Imaging System (magnification, 20×; Thermo Fisher Scientific, USA) with at least three fields of view per well.

In the GPX1 inhibitor assay, si-CXCL16 cells (SCC9 and SCC25) were inoculated in 6-well plates at 1.5×10^5 wells/well and cultured for 24 h with 2 μmol/L ED-71. Subsequently, the inhibitor-pretreated cells were inoculated at 5×10^4 cells/well in the upper chamber, and 600 μL of 10% FBS-DMEM/F12 was placed in the lower chamber. The cells were incubated, followed by formaldehyde fixation, crystal violet staining, and photographing.

2.7 Western blot

HNSCC cells from different groups were harvested using western blotting and immunoprecipitation (IP) lysis buffer (#P0013, Beyotime Institute of Biotechnology, China) supplemented with protease and phosphatase inhibitors, and then lysed on ice for 10 min. The total protein concentration was determined using a bicinchoninic acid (BCA) protein assay kit (Thermo Fisher Scientific). The protein samples were separated using sodium dodecyl sulfate-polyacrylamide gel electrophoresis (SDS-PAGE) precast Tris-Gly gels (4%–20% (1%=0.01 g/mL), #36270ES10, Yeasen Biotechnology, China) and then transferred to polyvinylidene fluoride (PVDF) membranes. The membranes were first incubated with 5% (volume fraction) milk (Beijing Sola Biotechnology Co., Ltd., China) for 1 h at room temperature, and then overnight at 4 °C with the following primary antibodies: anti-β-tublin (1:1000 (volume ratio, the same below); #AC030, ABclonal, China), anti-CXCL16 (1:1000; #60123-1-Ig, Proteintech, China), anti-*N*-cadherin (1:1000; #22018-1-AP, Proteintech), anti-*E*-cadherin (1:1000; #20874-1-AP, Proteintech), anti-NFE2L2 (1:1000; #80593-1-RR, Proteintech), anti-GPX1 (1:1000; #A6-C0-B9-R, Huabio, China), and anti-glyceraldehyde-3-phosphate dehydrogenase (anti-GAPDH; 1:1000; #60004-1-Ig, Proteintech). The membranes were washed three times and incubated with goat anti-rabbit immunoglobulin G (IgG) (1:3000; #A0208, Beyotime) or anti-mouse IgG (1:3000; #A0216, Beyotime) for 2 h at room temperature, and then analyzed using an FDbioDura ECL kit (FDbio Science, #FD8020, China) with a ChemiDoc-MP imager (Bio-Rad, USA).

2.8 RT-qPCR

Total cellular RNA was extracted using the TRIzol reagent (TaKaRa, Beijing, China) and its concentration was measured using a NanoDrop spectrophotometer (Thermo Fisher Scientific). The complementary DNA (cDNA) was obtained using the Evo M-MLV RT Premix Kit for reverse transcription-quantitative polymerase chain reaction (RT-qPCR) (#AG11706, Accurate Biotechnology (Hunan) Co., Ltd., China) with the reverse transcription performed at 37 °C for 15 min and at 85 °C for 5 s. A qPCR assay was performed using the Premix Pro Taq HS qPCR Kit (ROX Plus) (#AG11718, Accurate Biotechnology (Hunan) Co., Ltd.) with reagents provided in a protocol, yielding a total volume of 10 μL. The thermal cycling conditions were 95 °C for 1 min, followed by 40 cycles at 95 °C for 5 s and 60 °C for 30 s. Relative gene expression was determined by the $2^{-\Delta\Delta C_T}$ method using β-actin as an internal reference (Livak and Schmittgen, 2001), and the primers are listed in Table S2.

2.9 Measurement of intracellular ROS levels

Different groups of HNSCC cells (ED-71 final concentration of 10 μmol/L, DMEM/F12 without FBS) were incubated with 2,7-dichloro-hydroxyfluorescein diacetate (DCFH-DA; #T15458, TargetMol, USA) for 30 min at 37 °C in a dark environment and subsequently washed twice with DMEM/F12 without FBS. Photographs were taken randomly in the dark with at least three fields of view per well using the EVOS M7000 Smart Imaging System (magnification, 20×; Thermo Fisher Scientific).

2.10 Transcriptome gene analysis

SCC9 cells were cultured to achieve 70% confluency in 10-cm dishes and transfected with siRNA and Lipo3000 (Invitrogen) at a working concentration of 100 nmol/L. Cells were collected after 48 h and analyzed using RNA-sequencing (Lianchuan Biotech Co., Ltd., Hangzhou, China).

2.11 ELISA

The concentration of CXCL16 in the culture medium of HACAT, SCC9, and SCC25 cells was analyzed using the Human CXCL16 enzyme-linked immunosorbent assay (ELISA) Kit (#MM-2133H1, Jiangsu Meimian Industrial Co., Ltd., China). All assays were performed according to the manufacturer's protocol.

2.12 Statistical analysis

Experimental data were presented as mean±standard error of the mean (SEM). Overall survival (OS) was estimated using the Kaplan-Meier method. Differences between two groups were compared by the *t*-test. All experiments were performed with at least three replicates. Differences were considered significant when $P<0.05$. Statistical analyses were performed using GraphPad Prism 8 statistical software (GraphPad Software, USA).

3 Results

3.1 Overexpressed CXCL16 in HNSCC tissues and cell lines

In order to investigate the role of CXCL16 in tumor development in patients with HNSCC, the differences between HNSCC carcinoma and paracancer were analyzed using the TCGA database. The database was classified into a CXCL16 high-expression group (n=515) and low-expression group (n=44) according to the median level of CXCL16 in patients with HNSCC. The results revealed a significantly higher CXCL16 level in cancer tissues compared to adjacent normal tissues (Fig. 1a; $P<0.01$). To assess the diagnostic significance of high CXCL16 expression in patients with HNSCC, we conducted receiver operating characteristic (ROC) curve analysis and found that CXCL16 could statistically differentiate HNSCC tissues from normal tissues, with an area under the curve (AUC) of 0.6015 (95% confidence interval (CI): 0.5094–0.6937; $P<0.05$) (Fig. 1b). Subsequently, we evaluated the clinicopathological relationship between CXCL16 expression levels and HNSCC based on the primary tumor T-stage and the overall tumor stage. Each group was evaluated by comparing the two groups with the normal group. The findings demonstrated a positive correlation between high CXCL16 expression and advanced HNSCC tumor stage (Figs. 1c and 1d). The differential expression of CXCL16 did not differ significantly in terms of gender, distant metastasis, lymph node metastasis, or OS curves (Figs. S1a–1Sd). Next, we analyzed the relationship between the expression of CXCL16 and its clinical relevance in HNSCC tumors in the TCGA database, and found that high expression of CXCL16 in cancer tissues was correlated with age and lymphovascular invasion (Table S3). To verify CXCL16 expression in tissue cancer versus paracancer in patients with HNSCC, we randomly selected a paracancer case from the cut margin tissue of one patient with a negative pathology report, as well as eleven patients with HNSCC, all of whom underwent immunohistochemical staining for CXCL16. We found that CXCL16 expression was significantly upregulated in patients with HNSCC compared to normal tissues (Fig. 1e). In addition, we assessed CXCL16 expression in normal epidermal HACAT cell lines and HNSCC cell lines through qPCR and western blotting, confirming its positive expression in cancer cells (Figs. 1f and 1g). We analyzed the release of soluble CXCL16 in HACAT, SCC9, and SCC25 cell lines by ELISA and revealed that the expression trend of the HNSCC cell lines was slightly higher than that of the normal epithelial HACAT cell line (Fig. S1e). In addition, the receptor CXCR6 for CXCL16 was found to be highly expressed in HNSCC cell lines and tumor patient tissues by qPCR and immunohistochemistry (Figs. S1f and S1g).

3.2 Inhibition of proliferation, migration, and invasion in HNSCC cells by knockdown of *CXCL16*

In order to investigate the role of CXCL16 in HNSCC, we selected SCC9 and SCC25 cells with high CXCL16 expression as target cells and transfected them with si-CXCL16 to knock down the expression of CXCL16. The qPCR and western blotting results demonstrated that the knockdown efficiency of *CXCL16* was as expected (Figs. 2a and 2b). Furthermore, we compared the si-CXCL16 groups with the negative control (NC) group and analyzed the difference. *CXCL16* knockdown significantly affected the proliferation and clone formation of HNSCC cells (Figs. 2c and 2d). In addition, transwell experiments showed that migration and invasion were significantly inhibited in the *CXCL16* knockdown group compared with the NC group (Figs. 2e and 2f). Next, we continued to explore the effect of CXCL16 on the EMT process in SCC9 and SCC25 cells by western blotting experiments, and found that the knockdown of *CXCL16* inhibited EMT pathway transformation in SCC9 and SCC25 cell lines, the expression level of *N*-cadherin, a protein related to the EMT pathway, was reduced, and the expression level of *E*-cadherin was elevated (Fig. 2g).

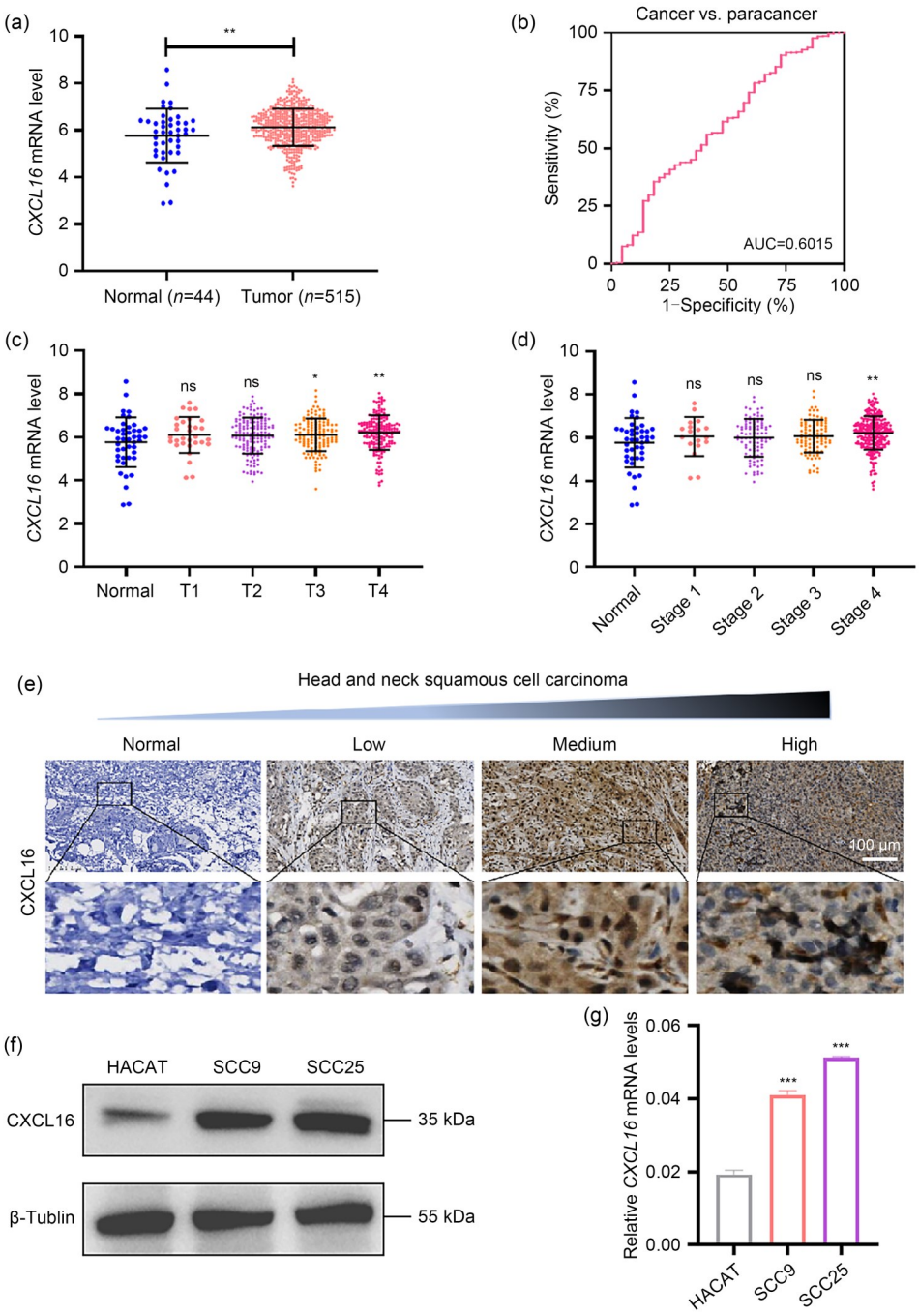

Fig. 1 Overexpressed CXCL16 in the tissues and cells of HNSCC patients. (a) Difference in mRNA expression levels of *CXCL16* between tumor tissues and adjacent normal tissues from the TCGA database. (b) The ROC curves showed that CXCL16 could effectively distinguish tumor tissue from adjacent normal tissues with an AUC of 0.6015. (c) Comparison of *CXCL16* expression levels in normal tissues with different T staging of tumor tissues from the TCGA database. (d) Comparison of *CXCL16* expression levels in normal tissues with different stages of tumor tissues from the TCGA database. (e) Immunohistochemical results of CXCL16 in tumor tissues and adjacent normal tissues of patients with HNSCC from our central hospital. (f) CXCL16 protein levels in normal epidermal cell line (HACAT) and HNSCC cell lines (SCC9 and SCC25). (g) Expression levels of *CXCL16* mRNA in normal epidermal cell line (HACAT) and HNSCC cell lines (SCC9 and SCC25). The data were expressed as mean±SEM, n=3. * P<0.05, ** P<0.01, *** P<0.001, vs. normal group. ns: no significance; CXCL16: CXC motif chemokine ligand 16; HNSCC: head and neck squamous cell carcinoma; mRNA: messenger RNA; TCGA: The Cancer Genome Atlas; ROC: receiver operating characteristic; AUC: area under curve; SEM: standard error of mean.

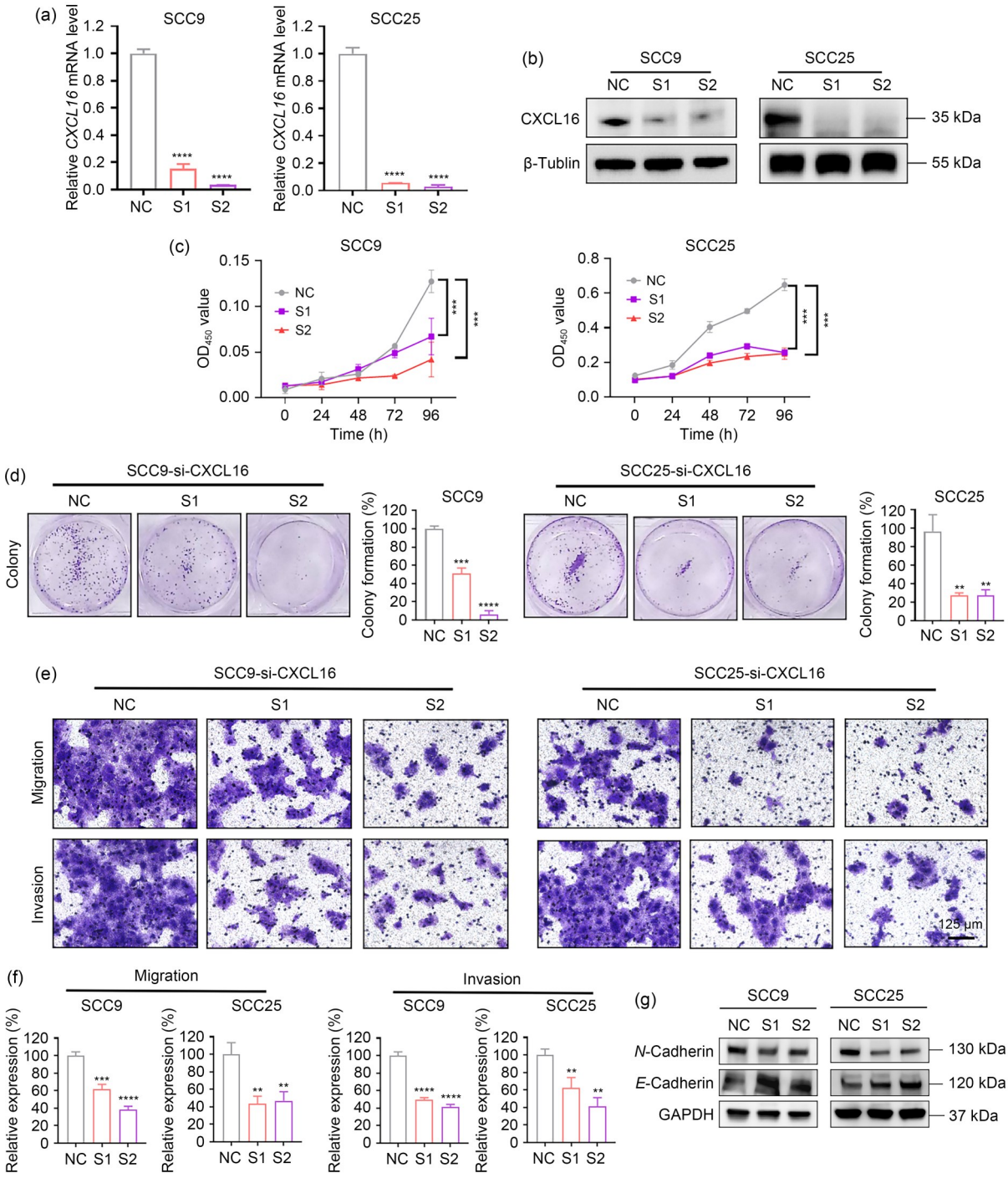

Fig. 2 Effects of CXCL16 on the proliferation, migration, and invasion of HNSCC cells. (a) mRNA level of *CXCL16* after its knockdown in HNSCC cell lines. (b) Protein level expression after *CXC16* knockdown in HNSCC cell lines. (c) Cell proliferation results (CCK8) of the NC group compared to si-CXCL16 groups. (d) Results of clone formation and quantification of SCC9 and SCC25 cell lines. (e) SCC9 and SCC25 cell migration and invasion results. (f) Quantification graphs of SCC9 and SCC25 cell migration and invasion. (g) Changes in EMT markers (*E*-cadherin and *N*-cadherin) in SCC9 and SCC25 cells after *CXCL16* knockdown. The data were expressed as mean±SEM, n=3. ** P<0.01, *** P<0.001, **** P<0.0001, vs. NC. CXCL16: CXC motif chemokine ligand 16; HNSCC: head and neck squamous cell carcinoma; mRNA: messenger RNA; CCK8: cell counting kit-8; NC: negative control; si-CXCL16: small interfering CXCL16; S1: si-CXCL16-1; S2: si-CXCL16-2; OD_{450}: optical density at 450 nm; GAPDH: glyceraldehyde-3-phosphate dehydrogenase; EMT: epithelial–mesenchymal transition; SEM: standard error of mean.

3.3 Promotion of HNSCC cell viability by CXCL16 through ROS action in the antioxidant pathway

In order to further explore the potential molecular mechanisms of CXCL16, we conducted RNA transcriptomic analysis of CXCL16 in HNSCC cells (Fig. 3a). The Gene Ontology (GO) pathway enrichment results showed a significant difference in antioxidant activity between the si-CXCL16 and NC groups (Fig. 3b). The analysis of differentially expressed genes revealed that urokinase-type plasminogen activator (*PLAU*), AXL receptor tyrosine kinase (*AXL*), *CXCL16*, processing of precursor 7 (*POP7*), intercellular adhesion molecule-1 (*ICAM1*), *GPX1*, ephrin receptor A2 (*EPHA2*), growth arrest-specific 6 (*GAS6*), integrin β4 (*ITGB4*), and borosilicate glass (*BSG*), associated with migratory invasion outcomes, were significantly downregulated in the si-CXCL16 group (Figs. 3c–3e). According to the results for protein–protein interaction (PPI) networks, *GPX1* acts as a downstream hub gene of *CXCL16* in regulating the migration and invasion of HNSCC cells (Fig. 3f).

To validate the results of transcriptome analysis, we compared the RNA levels of the si-CXCL16 groups with the NC group. The results showed significant downregulations of *PLAU*, *AXL*, *CXCL16*, *POP7*, *ICAM1*, *GPX1*, *EPHA2*, *GAS6*, *ITGB4*, and *BSG* in the si-CXCL16 groups, consistent with the transcriptome results (Fig. 4a). In addition, we randomly selected four unregulated genes from the transcriptome results and they were as expected based on qPCR (Fig. S2). Certain studies have confirmed that the antioxidant-related genes nuclear factor, erythroid 2-like 2 (*Nfe2l2*), superoxide dismutase 1 (*SOD1*), *SOD2*, glutathione reductase (*GSR*), nicotinamide adenine dinucleotide phosphate (NADPH) quinone oxidoreductase 1 (*NQO1*), glutathione synthetase (*GSS*), and glutamate-cysteine ligase modifier subunit (*GCLM*) play key roles in inflammatory responses and cancer development (Becker and Juvik, 2016; Mei XY et al., 2020; Wu et al., 2021; Tsai et al., 2022; Kassab et al., 2023). Our study also revealed that the mRNA levels of *Nfe2l2*, *SOD1*, *SOD2*, *GSR*, *NQO1*, *GSS*, and *GCLM* were significantly downregulated in the si-CXCL16 groups compared to the NC group (Figs. 4b and 4c). Western blotting experiments unveiled that the expression levels of GPX1 and NFE2L2 proteins were also downregulated in SCC9 and SCC25 cells (Figs. 4d). Furthermore, the trend of ROS upregulation was similar in SCC9 and SCC25 cell lines after *CXCL16* knockdown (Figs. 4e and 4f).

3.4 Promotion of HNSCC cell growth by CXCL16-GPX1 signaling way

In order to further verify that CXCL16 regulates HNSCC cell viability through GPX1, we used ED-71, a GPX1 inhibitor, combined with si-CXCL16-treated HNSCC cells. We compared the ED-71 and si-CXCL16 combination group with the si-CXCL16 alone group, and found that the combination of ED-71 and si-CXCL16 significantly inhibited the proliferation of SCC9 and SCC25 cells (Fig. 5a). In cell migration assays, it was also indicated that ED-71 combined with si-CXCL16 inhibited the migratory ability of HNSCC cell lines relative to the si-CXCL16 alone group (Figs. 5b and 5c). And through western blotting experiments, it was found that the combination of ED-71 and si-CXCL16 inhibited the transformation of EMT pathway in SCC9 and SCC25 cell lines, the expression level of EMT pathway-related protein *N*-cadherin decreased, and the expression level of *E*-cadherin increased (Fig. 5d). The clone formation results showed that the inhibition of GPX1 significantly suppressed cell clone formation (Figs. 5e, S3a, and S3b). We next verified the changes in mRNA levels of antioxidant genes in the ED-71 and si-CXCL16 combination group versus the si-CXCL16 alone group. *NQO1* and *GSR* levels were significantly downregulated, and the levels of *Nfe2l2* and *GSS* showed a downward trend (Fig. 5f). In addition, the ED-71 and si-CXCL16 combination group showed a similar trend towards the upregulation of ROS levels, indicating that knockdown of the expression of *CXCL16* inhibited the growth of HNSCC cells through the GPX1 signaling axis (Figs. 5g and 5h).

4 Discussion

HNSCC is a major malignant tumor characterized by high recurrence and metastasis rates. Therefore, identifying effective prognostic biomarkers and therapeutic targets for patients with HNSCC is of high urgency. Many clinical predictors of HNSCC are slowly coming into public view, and some researchers have developed bioinformatics tools for screening and evaluating prognostic biomarkers in HNSCC cohorts (Zhang et al., 2022). In addition to immune checkpoint inhibitor

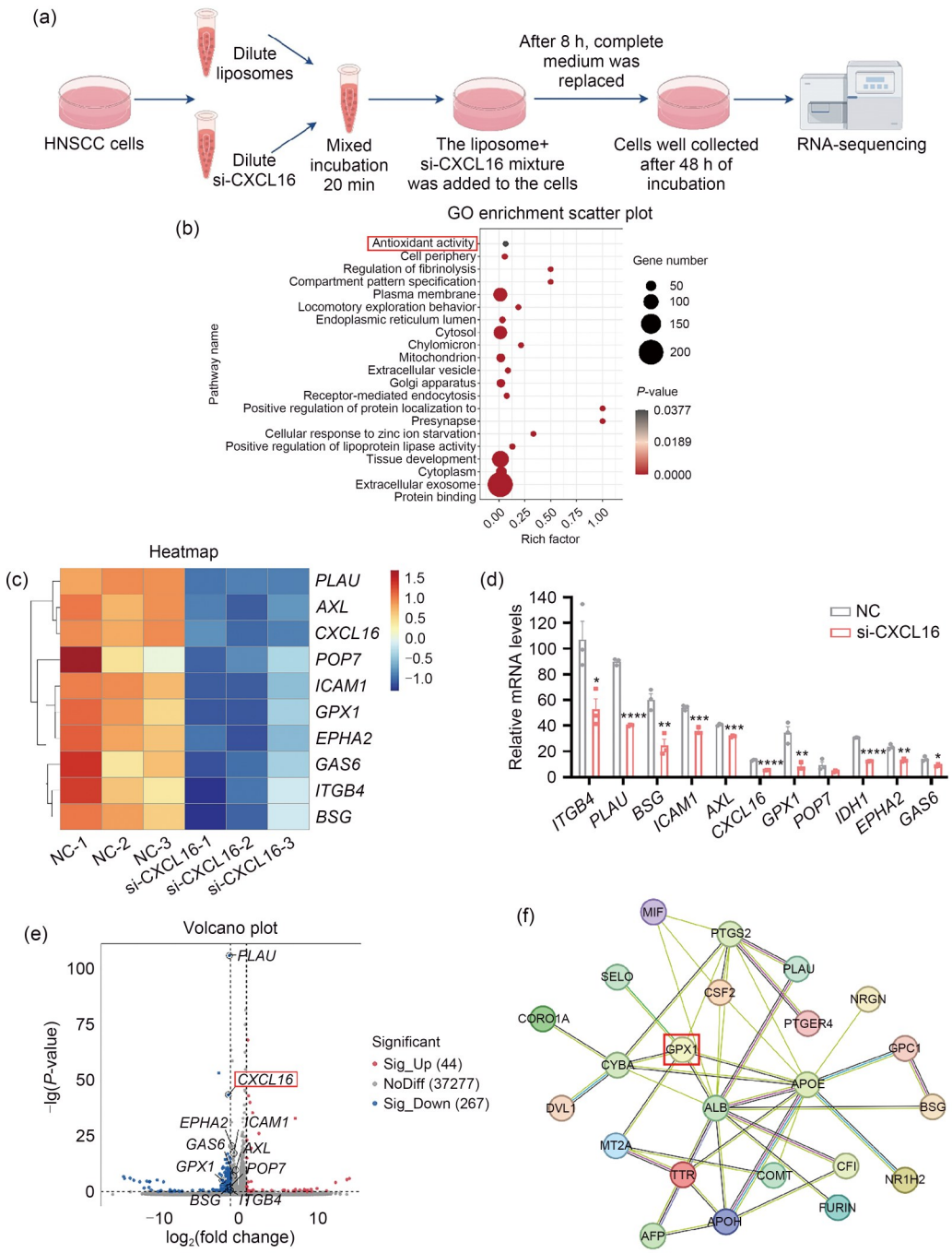

Fig. 3 Transcriptome sequencing analysis after knockdown of *CXCL16*. (a) Schematic diagram of the RNA-sequencing steps (created by Figdraw). (b) GO pathway enrichment analysis showed that the antioxidant pathway was enriched. (c) Differential gene expression heatmap (*PLAU*, *AXL*, *CXCL16*, *POP7*, *ICAM1*, *GPX1*, *EPHA2*, *GAS6*, *ITGB4*, and *BSG*). (d) Quantitative graph of differential gene expression. (e) Volcano plot showing differentially expressed genes of si-CXCL16 and NC. Upregulated genes (Sig_Up) and downregulated genes (Sig_Down) are marked in red and blue, respectively. (f) PPI network analysis showing the enrichment of antioxidant gene *GPX1*. The data were expressed as mean±SEM, n=3. * P<0.05, ** P<0.01, *** P<0.001, **** P<0.0001, vs. NC. CXCL16: CXC motif chemokine ligand 16; HNSCC: head and neck squamous cell carcinoma; GO: Gene Ontology; si-CXCL16: small interfering CXCL16; NC: negative control; PPI: protein–protein interaction; *ITGB4*: integrin β4; *PLAU*: urokinase-type plasminogen activator; *BSG*: borosilicate glass; *ICAM1*: intercellular adhesion molecule-1; *AXL*: AXL receptor tyrosine kinase; *GPX1*: glutathione peroxidase 1; *POP7*: processing of precursor 7; *IDH1*: isocitrate dehydrogenase 1; *EPHA2*: ephrin receptor A2; *GAS6*: growth arrest-specific 6; SEM: standard error of mean; NoDiff: no difference.

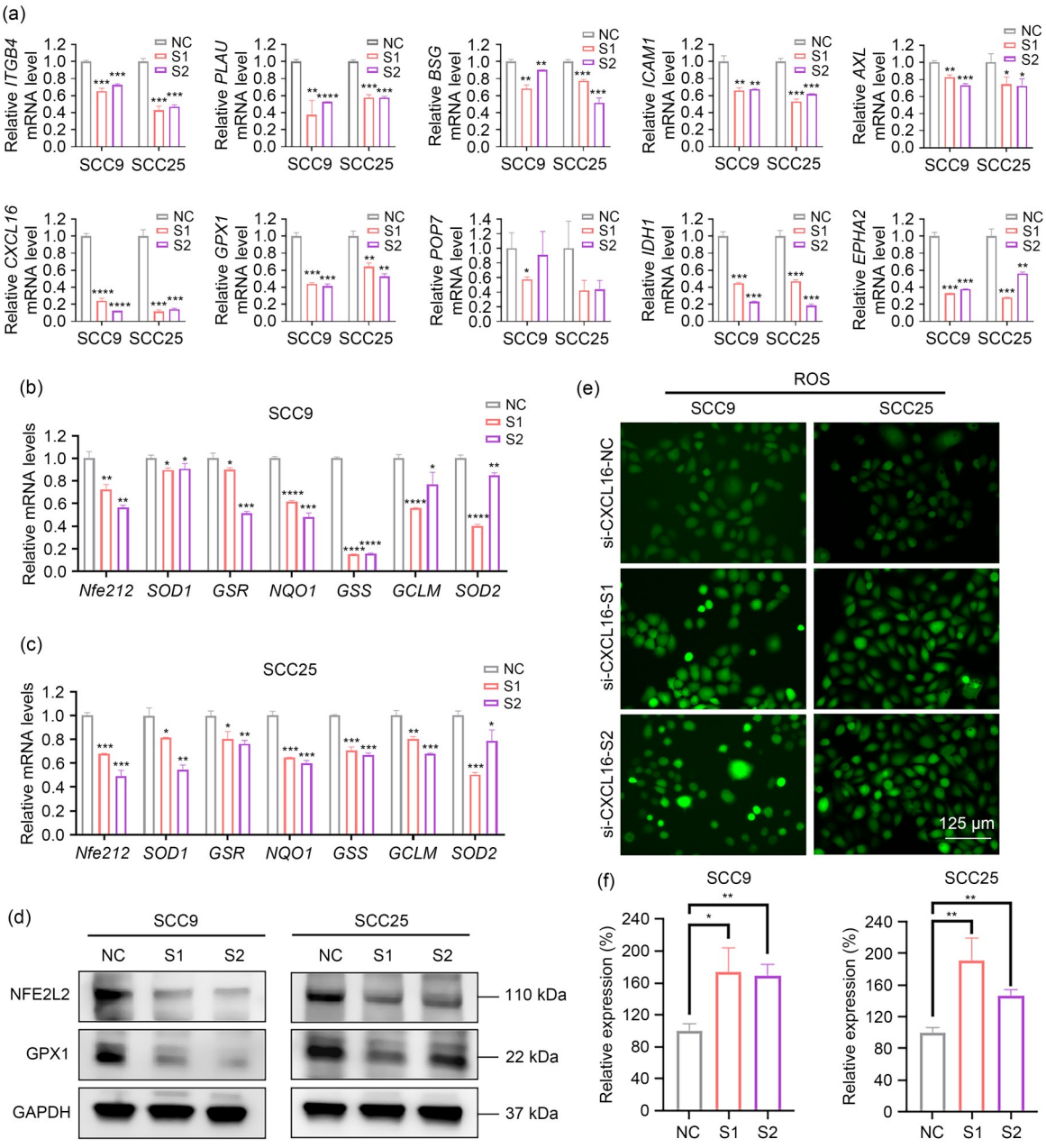

Fig. 4 Promotion of HNSCC development by CXCL16 via an antioxidant pathway. (a) The si-CXCL16 groups vs. the NC group were evaluated in a two-group comparison to validate the mRNA expression levels of differential genes associated with migration, invasion, and antioxidation. (b, c) The si-CXCL16 groups were compared with the NC group in the mRNA expression levels of antioxidant-related genes in SCC9 (b) and SCC25 (c) cells. (d) The protein levels of antioxidant-related genes GPX1 and NFE2L2 in SCC9 and SCC25 cell lines were changed after si-CXCL16 treatment. (e) ROS levels were significantly increased after the knockdown of *CXCL16* in SCC9 and SCC25 cell lines. (f) Quantitative graphs of ROS levels in SCC9 and SCC25 after the knockdown of *CXCL16*. The data were expressed as mean±SEM, n=3. * P<0.05, ** P<0.01, *** P<0.001, **** P<0.0001, vs. NC. HNSCC: head and neck squamous cell carcinoma; CXCL16: CXC motif chemokine ligand 16; si-CXCL16: small interfering CXCL16; mRNA: messenger RNA; NC: negative control; S1: si-CXCL16-1; S2: si-CXCL16-2; ROS: reactive oxygen species; *ITGB4*: integrin β4; *PLAU*: urokinase-type plasminogen activator; *BSG*: borosilicate glass; *ICAM1*: intercellular adhesion molecule-1; *AXL*: AXL receptor tyrosine kinase; *GPX1*: glutathione peroxidase 1; *POP7*: processing of precursor 7; *IDH1*: isocitrate dehydrogenase 1; *EPHA2*: ephrin receptor A2; *Nfe2l2*: nuclear factor, erythroid 2-like 2; *SOD*: superoxide dismutase; *GSR*: glutathione reductase; *GSS*: glutathione synthetase; *NQO1*: nicotinamide adenine dinucleotide phosphate (NADPH) quinone oxidoreductase 1; *GCLM*: glutamate-cysteine ligase modifier subunit; GAPDH: glyceraldehyde-3-phosphate dehydrogenase; SEM: standard error of mean.

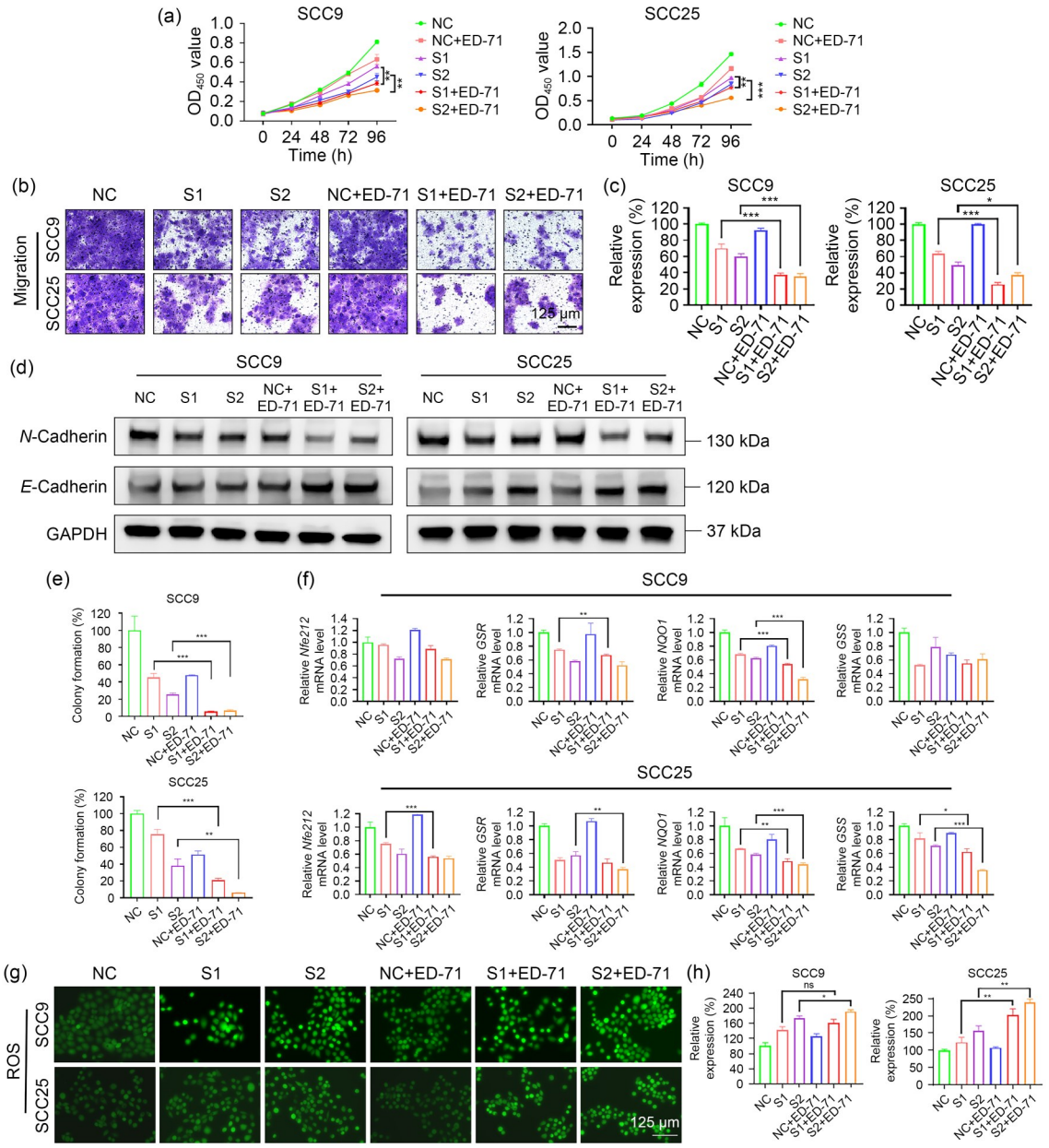

Fig. 5 Promotion of the development of HNSCC cells by CXCL16 through GPX1. (a) The ED-71 and si-CXCL16 combination group was compared with the si-CXCL16 alone group. The combination of ED-71 and si-CXCL16 inhibited the proliferation of HNSCC cells. (b) Migration inhibition results of ED-71 and si-CXCL16 on SCC9 and SCC25 cell lines after 48 h of cell incubation. (c) Quantification graphs of ED-71 and si-CXCL16 co-action migration. (d) Changes of EMT markers (*E*-cadherin and *N*-cadherin) in SCC9 and SCC25 cells after ED-71 and si-CXCL16 co-action. (e) Quantification graphs of clone formation in SCC9 and SCC25 cells after ED-71 and si-CXCL16 co-action. (f) The combination group of ED-71 and si-CXCL16 was compared with the si-CXCL16 alone group and the mRNA expression levels of antioxidant-related genes (*Nfe2l2*, *GSR*, *NQO1*, and *GSS*) were suppressed in HNSCC cells. (g) Increased ROS levels in SCC9 and SCC25 cell lines after the co-action of ED-71 and si-CXCL16. (h) Quantitative graphs of ROS levels in SCC9 and SCC25 cell lines after the co-action of ED-71 and si-CXCL16. The data were expressed as mean±SEM, n=3. ns: no significance; * P<0.05; ** P<0.01; *** P<0.001. HNSCC: head and neck squamous carcinoma; CXCL16: CXC motif chemokine ligand 16; GPX1: glutathione peroxidase 1; ED-71: eldecalcitol; si-CXCL16: small interfering CXCL16; NC: negative control; S1: si-CXCL16-1; S2: si-CXCL16-2; ROS: reactive oxygen species; mRNA: messenger RNA; *Nfe2l2*: nuclear factor, erythroid 2-like 2; *GSR*: glutathione reductase; *NQO1*: nicotinamide adenine dinucleotide phosphate (NADPH) quinone oxidoreductase 1; *GSS*: glutathione synthetase; GAPDH: glyceraldehyde-3-phosphate dehydrogenase; EMT: epithelial–mesenchymal transition; SEM: standard error of mean; OD_{450}: optical density at 450 nm.

treatment, other novel biomarker molecules have also been reported to be potential therapeutic targets, such as nuclear factor erythroid 2-related factor 2 (NRF2) and glycogen phosphorylase (PYGL), which are related to cellular metabolism (Tang et al., 2021; Guan et al., 2023). Although recent studies have shown significant progress in the genomic and immunotherapeutic aspects of HNSCC, few molecules can be applied in clinical practice (Gao et al., 2022; Ruffin et al., 2023). Consequently, surgery and radiotherapy remain the primary treatment options for HNSCC. In particular, the treatment of advanced HNSCC in the course of clinical treatment has been associated with a high rate of resistance, which frequently leads to recurrence and poor therapeutic effects in HNSCC (Jiang et al., 2022). As understood, chemokines play an important role as mediators of intercellular communication, as they can recruit immune cells to generate an immune response, regulate tumor cells' migration and invasion, and influence tumor development (Liu et al., 2020; Khan et al., 2022). Among these, CXCL16 plays a vital role in angiogenesis, the tumor immune microenvironment, and the promotion of tumor cells' proliferation, migration, invasion, metastasis, and EMT transformations (Korbecki et al., 2021). CXCL16 was found to cause kidney damage and cardiovascular disease; elevated CXCL16 levels promoted the development of prostate cancer (Izquierdo et al., 2014; Richardsen et al., 2015). Moreover, it has been found that the CXCL16-CXCR6 signaling axis induces the migration and invasion of colorectal cancer and osteosarcoma cells, and promotes the transformation of the EMT pathway. Osteosarcoma predominantly arises from activation of CXCR6 via the protein kinase B (AKT) pathway (Matsushita et al., 2012; Ma et al., 2017). However, the biological function and molecular mechanism of CXCL16 in HNSCC are still unclear.

Our study established that the expression of CXCL16 was upregulated in HNSCC patients through TCGA database analysis (Fig. 1a). We also observed that high expression of CXCL16 was positively correlated with tumor T3 and T4 stages (Fig. 1c). ROC curve analysis revealed that high CXCL16 expression effectively distinguished HNSCC from individuals without malignancy (Fig. 1b). To validate the veracity of the cancer database, we examined CXCL16 expression in patient tissues and HNSCC cell lines, yielding results that consistently align with the database predictions (Figs. 1e–1g). Subsequently, we investigated the role of CXCL16 in HNSCC cells and utilized siRNA to knock down *CXCL16* expression in these cells. The knockdown of *CXCL16* inhibited the migration and invasion of HNSCC cells (Fig. 2), indicating that CXCL16 may be a promising candidate target molecule for HNSCC patients.

Further transcriptome analysis indicated that the cellular antioxidant pathway was altered, and the antioxidant-related gene *GPX1* was downregulated (Fig. 3d). According to previous reports, GPX1 interacts with superoxide dismutase and catalase to form an enzymatic antioxidant system that reduces ROS and limits their toxicity. It can be involved in tumor biology through various pathways such as cell proliferation, apoptosis, invasion, and immune response (Zhao et al., 2022; Pei et al., 2023). Upregulation of GPX1 expression has been demonstrated to correlate with a poor prognosis in glioblastoma, and both cellular GPX1 and exosomal GPX1 have been identified as critical for controlling hydrogen peroxide homeostasis and attenuating oxidative stress in hypoxic glioblastoma (Lei et al., 2023). In hepatocellular carcinoma, reduced selenium-binding protein 1 promotes hepatocellular carcinoma invasion by enhancing GPX1 activity and decreasing hypoxia-inducible factor-1α (HIF-1α) expression (Huang et al., 2012). Herein, we used ED-71 (GPX1 inhibitor) in combination with si-CXCL16 to treat HNSCC cells and verify the effect of CXCL16 on the viability of HNSCC cells via GPX1 (Fig. 5). ROS accumulation causes DNA damage, genetic instability, metabolic adaptation, drug resistance, and cell death (Moloney and Cotter, 2018). According to our experimental results, knockdown of *CXCL16* expression affected the increase in ROS levels in HNSCC cells by regulating the level of GPX1, resulting in a diminished ability of cells to undergo proliferation, migration, and invasion.

5 Conclusions

In summary, our results indicate that CXCL16 is highly expressed in the HNSCC tissues and is associated with a poor prognosis. In terms of the underlying mechanism, elevated CXCL16 expression promotes the migration and invasion ability of HNSCC cells by regulating the level of antioxidant gene *GPX1* (Fig. 6). Our

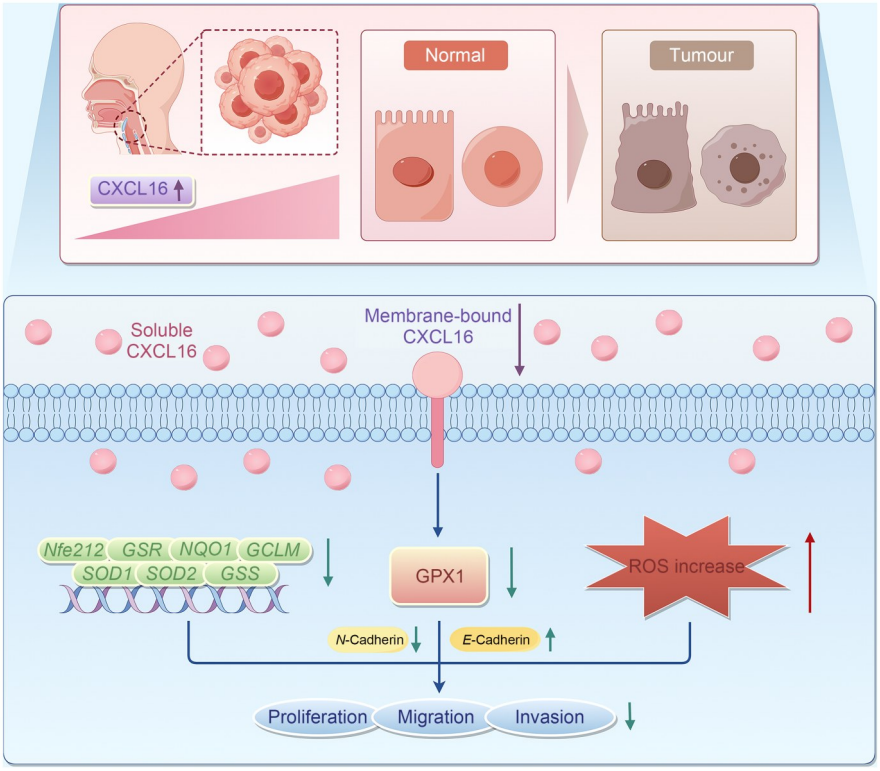

Fig. 6 Schematic representation of CXCL16 promoting HNSCC development through GPX1 (created by Figdraw). CXCL16 promotes HNSCC tumor development by regulating GPX1-mediated antioxidant levels. CXCL16: CXC motif chemokine ligand 16; HNSCC: head and neck squamous cell carcinoma; GPX1: glutathione peroxidase 1; *Nfe2l2*: nuclear factor, erythroid 2-like 2; *SOD*: superoxide dismutase; *GSR*: glutathione reductase; *GSS*: glutathione synthetase; *NQO1*: nicotinamide adenine dinucleotide phosphate (NADPH) quinone oxidoreductase 1; GCLM: glutamate-cysteine ligase modifier subunit; ROS: reactive oxygen species.

study provides a new direction for treating HNSCC and highlights the potential value of CXCL16 as a new diagnostic target for HNSCC.

Data availability statement

All datasets analyzed in this study are available from the corresponding author upon request.

Acknowledgments

This work was supported by the Scientific Research Fund of the National Health Commission-Zhejiang Provincial Health Major Science and Technology Plan Project (No. WKJ-ZJ-2415), the Key Research and Development Program of Zhejiang Province (No. 2024C03166), the Traditional Chinese Medicine Science and Technology Project of Zhejiang Province (No. 2022ZB020), and the Zhejiang Provincial Natural Science Foundation of China (No. LY21H160049). We also thank Figdraw (https://www.figdraw.com) for the assistance in creating scheme.

Author contributions

All authors contributed to the study's conception and design. Ru HE and Hongyi JIANG designed the experiment and drafted the manuscript. Chengchi ZHANG, Yuan CHEN, Wenshun LIU, Yunye LIU, Yining ZHANG, and Chengying SHAO performed the study. Xinyue DENG, Xiaozheng ZHU, and Chuanming ZHENG analyzed data. Yanting DUAN and Jiajie XU designed the experiment, revised the manuscript, and monitored the project progression. All authors have read and approved the final manuscript, and therefore, have full access to all the data in the study and take responsibility for the integrity and security of the data.

Compliance with ethics guidelines

Ru HE, Hongyi JIANG, Chengchi ZHANG, Yuan CHEN, Wenshun LIU, Xinyue DENG, Xiaozheng ZHU, Yunye LIU, Chuanming ZHENG, Yining ZHANG, Chengying SHAO, Yanting DUAN, and Jiajie XU declare that they have no conflicts of interest.

All patients were informed of sample collection and use. Tissue samples were collected and used according to the protocols approved by the Human Research Ethics Committee of Zhejiang Provincial People's Hospital (No. QT2024066). This study was conducted in accordance with the Declaration of Helsinki and national and international guidelines.

References

Abel S, Hundhausen C, Mentlein R, et al., 2004. The transmembrane CXC-chemokine ligand 16 is induced by IFN-γ and TNF-α and shed by the activity of the disintegrin-like metalloproteinase ADAM10. *J Immunol*, 172(10):6362-6372. https://doi.org/10.4049/jimmunol.172.10.6362

Becker TM, Juvik JA, 2016. The role of glucosinolate hydrolysis products from brassica vegetable consumption in inducing antioxidant activity and reducing cancer incidence. *Diseases*, 4(2):22. https://doi.org/10.3390/diseases4020022

Bray F, Ferlay J, Soerjomataram I, et al., 2018. Global cancer statistics 2018: GLOBOCAN estimates of incidence and mortality worldwide for 36 cancers in 185 countries. *CA Cancer J Clin*, 68(6):394-424. https://doi.org/10.3322/caac.21492

Brockstein B, Haraf DJ, Rademaker AW, et al., 2004. Patterns of failure, prognostic factors and survival in locoregionally advanced head and neck cancer treated with concomitant chemoradiotherapy: a 9-year, 337-patient, multiinstitutional experience. *Ann Oncol*, 15(8):1179-1186. https://doi.org/10.1093/annonc/mdh308

Chalabi-Dchar M, Cassant-Sourdy S, Duluc C, et al., 2015. Loss of somatostatin receptor subtype 2 promotes growth of KRAS-induced pancreatic tumors in mice by activating PI3K signaling and overexpression of CXCL16. *Gastroenterology*, 148(7):1452-1465. https://doi.org/10.1053/j.gastro.2015.02.009

Cho SW, Kim YA, Sun HJ, et al., 2016. CXCL16 signaling mediated macrophage effects on tumor invasion of papillary thyroid carcinoma. *Endocr Relat Cancer*, 23(2):113-124. https://doi.org/10.1530/ERC-15-0196

Collado A, Marques P, Escudero P, et al., 2018. Functional role of endothelial CXCL16/CXCR6-platelet-leucocyte axis in angiotensin II-associated metabolic disorders. *Cardiovasc Res*, 114(13):1764-1775. https://doi.org/10.1093/cvr/cvy135

Dequanter D, Dok R, Koolen L, et al., 2017. Prognostic significance of glutathione peroxidase levels (GPx1) in head and neck cancers. *Front Oncol*, 7:84. https://doi.org/10.3389/fonc.2017.00084

Fan S, Tang QL, Lin YJ, et al., 2011. A review of clinical and histological parameters associated with contralateral neck metastases in oral squamous cell carcinoma. *Int J Oral Sci*, 3(4):180-191. https://doi.org/10.4248/IJOS11068

Gao ZR, Ling XY, Shi CY, et al., 2022. Tumor immune checkpoints and their associated inhibitors. *J Zhejiang Univ-Sci B (Biomed & Biotechnol)*, 23(10):823-843. https://doi.org/10.1631/jzus.B2200195

Griffith JW, Sokol CL, Luster AD, 2014. Chemokines and chemokine receptors: positioning cells for host defense and immunity. *Annu Rev Immunol*, 32:659-702. https://doi.org/10.1146/annurev-immunol-032713-120145

Guan JZ, Xu X, Qiu G, et al., 2023. Cellular hierarchy framework based on single-cell/multi-patient sample sequencing reveals metabolic biomarker *PYGL* as a therapeutic target for HNSCC. *J Exp Clin Cancer Res*, 42:162. https://doi.org/10.1186/s13046-023-02734-w

Han J, Fu RJ, Chen C, et al., 2021. CXCL16 promotes gastric cancer tumorigenesis via ADAM10-dependent CXCL16/CXCR6 axis and activates Akt and MAPK signaling pathways. *Int J Biol Sci*, 17(11):2841-2852. https://doi.org/10.7150/ijbs.57826

Hattermann K, Gebhardt H, Krossa S, et al., 2016. Transmembrane chemokines act as receptors in a novel mechanism termed inverse signaling. *eLife*, 5:e10820. https://doi.org/10.7554/eLife.10820

Hsieh CY, Lin CC, Huang YW, et al., 2022. Macrophage secretory IL-1β promotes docetaxel resistance in head and neck squamous carcinoma via SOD2/CAT-ICAM1 signaling. *JCI Insight*, 7(23):e157285. https://doi.org/10.1172/jci.insight.157285

Hu WD, Liu Y, Zhou WH, et al., 2014. CXCL16 and CXCR6 are coexpressed in human lung cancer *in vivo* and mediate the invasion of lung cancer cell lines *in vitro*. *PLoS ONE*, 9(6):e99056. https://doi.org/10.1371/journal.pone.0099056

Huang C, Ding GY, Gu CY, et al., 2012. Decreased selenium-binding protein 1 enhances glutathione peroxidase 1 activity and downregulates HIF-1α to promote hepatocellular carcinoma invasiveness. *Clin Cancer Res*, 18(11):3042-3053. https://doi.org/10.1158/1078-0432.CCR-12-0183

Izquierdo MC, Martin-Cleary C, Fernandez-Fernandez B, et al., 2014. CXCL16 in kidney and cardiovascular injury. *Cytokine Growth Factor Rev*, 25(3):317-325. https://doi.org/10.1016/j.cytogfr.2014.04.002

Jiang YY, Guo HY, Tong T, et al., 2022. lncRNA lnc-POP1-1 upregulated by VN1R5 promotes cisplatin resistance in head and neck squamous cell carcinoma through interaction with MCM5. *Mol Ther*, 30(1):448-467. https://doi.org/10.1016/j.ymthe.2021.06.006

Karaki S, Blanc C, Tran T, et al., 2021. CXCR6 deficiency impairs cancer vaccine efficacy and $CD8^+$ resident memory T-cell recruitment in head and neck and lung tumors. *J Immunother Cancer*, 9(3):e001948. https://doi.org/10.1136/jitc-2020-001948

Kassab RB, Elhenawy AA, AbdulrahmanTheyab, et al., 2023. Modulation of inflammatory, oxidative, and apoptotic stresses mediates the renoprotective effect of daidzein against glycerol-induced acute kidney injury in rats. *Environ Sci Pollut Res Int*, 30(56):119016-119033. https://doi.org/10.1007/s11356-023-30461-4

Khan P, Fatima M, Khan MA, et al., 2022. Emerging role of chemokines in small cell lung cancer: road signs for metastasis, heterogeneity, and immune response. *Semin Cancer Biol*, 87:117-126. https://doi.org/10.1016/j.semcancer.2022.11.005

Kim MJ, Sun HJ, Song YS, et al., 2019. CXCL16 positively correlated with M2-macrophage infiltration, enhanced angiogenesis, and poor prognosis in thyroid cancer. *Sci Rep*, 9:13288. https://doi.org/10.1038/s41598-019-49613-z

Korbecki J, Bajdak-Rusinek K, Kupnicka P, et al., 2021. The role of CXCL16 in the pathogenesis of cancer and other

diseases. *Int J Mol Sci*, 22(7):3490. https://doi.org/10.3390/ijms22073490

Lei FJ, Chiang JY, Chang HJ, et al., 2023. Cellular and exosomal GPx1 are essential for controlling hydrogen peroxide balance and alleviating oxidative stress in hypoxic glioblastoma. *Redox Biol*, 65:102831. https://doi.org/10.1016/j.redox.2023.102831

Lepore F, D'Alessandro G, Antonangeli F, et al., 2018. CXCL16/CXCR6 axis drives microglia/macrophages phenotype in physiological conditions and plays a crucial role in glioma. *Front Immunol*, 9:2750. https://doi.org/10.3389/fimmu.2018.02750

Liu H, Yang ZJ, Lu WP, et al., 2020. Chemokines and chemokine receptors: a new strategy for breast cancer therapy. *Cancer Med*, 9(11):3786-3799. https://doi.org/10.1002/cam4.3014

Liu HY, Wang GQ, Wu T, et al., 2022. Efficacy and safety of eldecalcitol for osteoporosis: a meta-analysis of randomized controlled trials. *Front Endocrinol (Lausanne)*, 13:854439. https://doi.org/10.3389/fendo.2022.854439

Livak KJ, Schmittgen TD, 2001. Analysis of relative gene expression data using real-time quantitative PCR and the $2^{-\Delta\Delta C_T}$ method. *Methods*, 25(4):402-408. https://doi.org/10.1006/meth.2001.1262

Lu YP, Kou YY, Gao Y, et al., 2023. Eldecalcitol inhibits the progression of oral cancer by suppressing the expression of GPx-1. *Oral Dis*, 29(2):615-627. https://doi.org/10.1111/odi.14010

Ma YS, Xu X, Luo M, 2017. CXCR6 promotes tumor cell proliferation and metastasis in osteosarcoma through the Akt pathway. *Cell Immunol*, 311:80-85. https://doi.org/10.1016/j.cellimm.2016.11.001

Matloubian M, David A, Engel S, et al., 2000. A transmembrane CXC chemokine is a ligand for HIV-coreceptor Bonzo. *Nat Immunol*, 1(4):298-304. https://doi.org/10.1038/79738

Matsushita K, Toiyama Y, Tanaka K, et al., 2012. Soluble CXCL16 in preoperative serum is a novel prognostic marker and predicts recurrence of liver metastases in colorectal cancer patients. *Ann Surg Oncol*, 19(Suppl 3):518-527. https://doi.org/10.1245/s10434-011-1993-8

Mei XY, Qi DS, Zhang T, et al., 2020. Inhibiting MARSs reduces hyperhomocysteinemia-associated neural tube and congenital heart defects. *EMBO Mol Med*, 12(3):e9469. https://doi.org/10.15252/emmm.201809469

Mei Z, Huang JW, Qiao B, et al., 2020. Immune checkpoint pathways in immunotherapy for head and neck squamous cell carcinoma. *Int J Oral Sci*, 12:16. https://doi.org/10.1038/s41368-020-0084-8

Moloney JN, Cotter TG, 2018. ROS signalling in the biology of cancer. *Semin Cell Dev Biol*, 80:50-64. https://doi.org/10.1016/j.semcdb.2017.05.023

Moreira D, Sampath S, Won H, et al., 2021. Myeloid cell-targeted STAT3 inhibition sensitizes head and neck cancers to radiotherapy and T cell-mediated immunity. *J Clin Invest*, 131(2):e137001. https://doi.org/10.1172/JCI137001

Pei J, Pan XY, Wei GH, et al., 2023. Research progress of glutathione peroxidase family (GPX) in redoxidation. *Front Pharmacol*, 14:1147414. https://doi.org/10.3389/fphar.2023.1147414

Richardsen E, Ness N, Melbø-Jørgensen C, et al., 2015. The prognostic significance of CXCL16 and its receptor C-X-C chemokine receptor 6 in prostate cancer. *Am J Pathol*, 185(10):2722-2730. https://doi.org/10.1016/j.ajpath.2015.06.013

Ruffin AT, Li H, Vujanovic L, et al., 2023. Improving head and neck cancer therapies by immunomodulation of the tumour microenvironment. *Nat Rev Cancer*, 23(3):173-188. https://doi.org/10.1038/s41568-022-00531-9

Saddawi-Konefka R, O'Farrell A, Faraji F, et al., 2022. Lymphatic-preserving treatment sequencing with immune checkpoint inhibition unleashes cDC1-dependent antitumor immunity in HNSCC. *Nat Commun*, 13:4298. https://doi.org/10.1038/s41467-022-31941-w

Siegel RL, Miller KD, Jemal A, 2020. Cancer statistics, 2020. *CA Cancer J Clin*, 70(1):7-30. https://doi.org/10.3322/caac.21590

Siu LL, Even C, Mesía R, et al., 2019. Safety and efficacy of durvalumab with or without tremelimumab in patients with PD-L1-low/negative recurrent or metastatic HNSCC: the phase 2 CONDOR randomized clinical trial. *JAMA Oncol*, 5(2):195-203. https://doi.org/10.1001/jamaoncol.2018.4628

Tang YC, Hsiao JR, Jiang SS, et al., 2021. c-MYC-directed NRF2 drives malignant progression of head and neck cancer via glucose-6-phosphate dehydrogenase and transketolase activation. *Theranostics*, 11(11):5232-5247. https://doi.org/10.7150/thno.53417

Tsai CF, Chen GW, Chen YC, et al., 2022. Regulatory effects of quercetin on M1/M2 macrophage polarization and oxidative/antioxidative balance. *Nutrients*, 14(1):67. https://doi.org/10.3390/nu14010067

Wu W, Geng ZX, Bai HR, et al., 2021. Ammonium ferric citrate induced ferroptosis in non-small-cell lung carcinoma through the inhibition of GPX4-GSS/GSR-GGT axis activity. *Int J Med Sci*, 18(8):1899-1909. https://doi.org/10.7150/ijms.54860

Zhang GS, Wang Q, Qi XL, et al., 2022. OShnscc: a novel user-friendly online survival analysis tool for head and neck squamous cell carcinoma based on RNA expression profiles and long-term survival information. *J Zhejiang Univ-Sci B (Biomed & Biotechnol)*, 23(3):249-257. https://doi.org/10.1631/jzus.B2100512

Zhao YJ, Wang H, Zhou JD, et al., 2022. Glutathione peroxidase GPX1 and its dichotomous roles in cancer. *Cancers (Basel)*, 14(10):2560. https://doi.org/10.3390/cancers14102560

Supplementary information

Tables S1–S3; Figs. S1–S3